Pure Appl. Chem., Vol. 72, Nos. 1–2, pp. 179–188, 2000.

Chemistry and photophysics of thiol-stabilized II-VI semiconductor nanocrystals*

Alexander Eychmüller† and Andrey L. Rogach§

University of Hamburg, Institute for Physical Chemistry, Bundesstr. 45, D-20146 Hamburg

Abstract: The chemical and physical properties of thiol-stabilized semiconductor nanocrystals are reviewed. The materials prepared include cadmium and mercury chalcogenides with sizes ranging between 1.4 and about 8 nm. In this size regime, the optical properties of the particles are governed by the size-quantization effect. All nanocrystals synthesized belong to the cubic crystal structure. Some applications of this class of materials are outlined.

INTRODUCTION

Composing of superstructures from nanocrystals is one of the most interesting branches of today's nanoscience. A prerequisite for successful attempts in this direction is the availability of nanoparticles of superior quality. "Quality" in this respect is expressed in terms of monodispersity, surface control, stability, and variability in composition.

Thiol-stabilized II-VI semiconductor particles have proven to fulfill these requirements to a large extent. Nanoparticles of different materials (CdS, CdSe, CdTe, and HgTe) have been prepared with several different thiols giving the opportunity to vary the functional groups at the surfaces and, thus, regulating the chemical behavior of the particles. This opens the field of doing chemistry with the preformed particles. This could be the built-up of larger structures consisting of nanocrystals of one kind, "hetero-atomic" structures made from different semiconductor materials, or even the connection of semiconductor and metal particles.

Since the first paper on CdS nanocrystals in 1994 [1] our group has published some 20 articles on the synthesis, characterization, structure and photophysics of thiol-stabilized II-VI semiconductor particles. This work will be reviewed comprehensively on the following pages. First, we will outline the general synthetic route and give some examples of standard characterization. Some deeper insight into structural and photophysical properties of selected nanocrystal species will be given in the third paragraph, whereas the last section is devoted to the first steps undertaken into the direction of applications of this class of nanostructures.

SYNTHESIS AND CHARACTERIZATION

The general synthetic process follows a similar route for all nanocrystals: a metal salt is dissolved in water in the presence of the stabilizing thiol. The basic solution is purged by inert gas before the chalcogen source is injected. The compounds prepared so far include CdS [1], CdSe [2], CdTe [3,4,5], HgSe [6], HgTe [7], and CdHgTe [8]. The thiols used were 1-thioglycerol, 2-mercaptoethanol, 1-mercapto-2-propanol, 1,2-dimercapto-3-propanol, thioglycolic acid, thiolactic acid, and cysteamin [9]. Subsequent

Pure Appl. Chem.* **72, 1–331 (2000). An issue of reviews and research papers based on lectures presented at the 1st IUPAC Workshop on Advanced Materials (WAM1), Hong Kong, July 1999, on the theme of nanostructured systems.
†Corresponding author
§On leave from the Physico-Chemical Research Institute, Belarussian State University, Leningradskaya 14, 220050 Minsk, Belarus

to the first steps in the preparation, heating of the reaction solution may be applied in order to initiate particle growth. Thus, this preparative approach relies on the separation of nucleation and growth very similar to the extremely successful "TOP/TOPO (tri–octyl phosphine/tri–octyl phosphine oxide) preparation" of II-VI and III-V semiconductor nanoparticles [10,11]. Yet another similarity between the two strategies is the postpreparative treatment by applying size-selective precipitation to the crude cluster solutions [12]. The sizes of the evolving nanocrystals depend mainly on the concentration ratios of the chemicals involved and on the duration of the heat treatment.

As an example, and in order to get a sense of the precise preparative conditions, let us focus on the recently published preparation of very small CdSe nanocrystals [2]: A solution of 1.97 g (4.70 mmol) of $Cd(ClO_4)_2 \cdot 6H_2O$ and 11.54 mmol of the stabilizer (RSH) in 250 mL of demineralized water was adjusted to pH 11.2 with 1 M NaOH. The solution was placed in a three-necked flask fitted with a septum and valves and was deaerated with N_2 bubbling for 30 min. Under vigorous stirring, 44 mL (2.2 mmol) of the freshly prepared oxygen-free 0.05 M NaHSe solution was injected. The initial molar ratio Cd^{2+}:Se^{2-}:RSH was therefore app. 1:0.5:2.4, which were the same conditions used for the preparation of thiol-stabilized CdS [1] and CdTe [3,4] nanoclusters. The addition of NaHSe produced bright yellow, transparent colloids stable towards oxidation under air. Solutions were refluxed for different times (up to 12 h), and aliquots were removed at regular intervals (15–30 min) with absorption spectra taken to monitor the growth of the clusters. The development of absorption spectra of thioalcohol-stabilized CdSe nanoparticles with time resembles that of thioalcohol-stabilized CdS and CdTe nanoparticles [1,3,4]. Addition of the NaHSe solution caused the appearance of absorption shoulders or maxima in the UV region and unstructured absorption features at longer wavelengths. The heating of the solutions led to an increase of absorption between 330 and 400 nm at the expense of the short wavelength bands. New absorption maxima appeared at specific wavelengths, suggesting the formation of some thermodynamically favorable cluster structures. A prolonged refluxing (up to 12 h) caused a continuous red shift of the absorption edge up to 450 nm, which was not accompanied by a formation of new pronounced absorption maxima. Particle growth occurred continuously at this stage via Ostwald ripening. Absorption spectra of the crude colloidal solutions represented a mixture of CdSe nanoparticles with different sizes. The method of size-selective precipitation [12] was used to isolate the samples of CdSe nanoparticles with different sizes and narrow size distributions from crude solutions. They were concentrated down to app. 30 mL using a rotary evaporator, and 2-propanol was added dropwise until turbidity occurred. The solutions were stirred for 2–3 h and precipitate and supernatant were separated through centrifugation.

In Fig.1 we summarized the absorption spectra of (from left to right) size-selected samples of CdS, CdSe and CdTe nanocrystals. Two fractions of each material are shown. All samples display clearly resolved electronic transitions, the positions of which are strongly shifted to higher energies as compared to the bandgaps of the respective bulk materials. This "quantum size effect" has been observed in many laboratories for almost all semiconductor materials and can be considered as being well understood [13,14].

The two CdS species shown in Fig.1 are peculiar in a sense that their superior quality allows crystallization of these nanoparticles into superstructures [15,16,17].

As examples for standard characterizations of nanoparticles we show some results from nanosized HgTe particles [7]. Figure 2 shows the powder X-ray diffraction pattern (P-XRD) of a fraction of HgTe nanoparticles. The crystalline structure derived from the positions of the wide-angle diffraction peaks clearly indicates a cubic (coloradoite) HgTe phase. The wide-angle diffraction peaks are broadened due to the small particle size. The mean cluster sizes estimated from the full width at half-maximum intensity of the (111) reflection, according to the Scherrer equation, gives a value of about 3.5 nm [18]. The weakly resolved small-angle X-ray diffraction peak indicates a rather broad size distribution of HgTe nanocrystals in aqueous colloidal solution. In order to determine the size, shape and crystal structure of

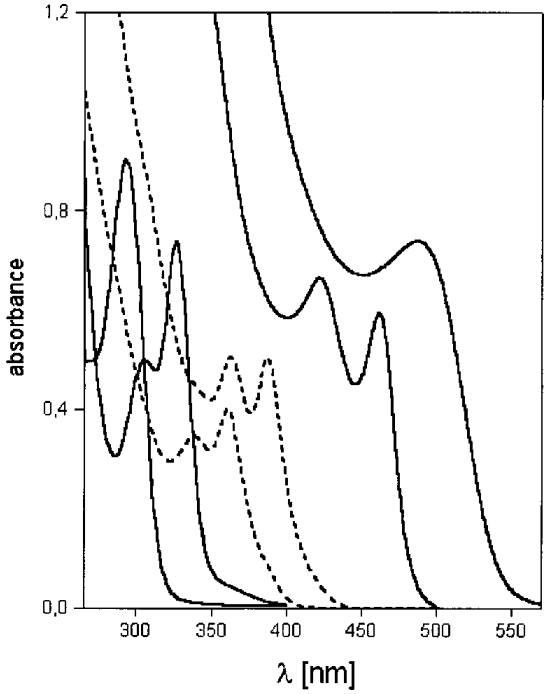

Fig. 1 Absorption spectra of very small cadmium chalcogenide nanocrystals, from left: two samples of CdS, two samples of CdSe, two samples of CdTe.

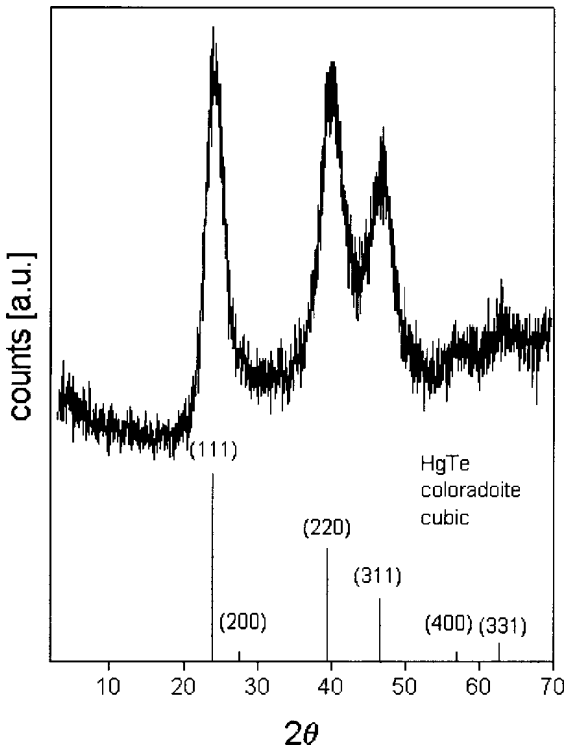

Fig. 2 Powder X-ray diffractogram of HgTe nanocrystals. The line spectrum gives the bulk HgTe coloradoite reflections with their relative intensities.

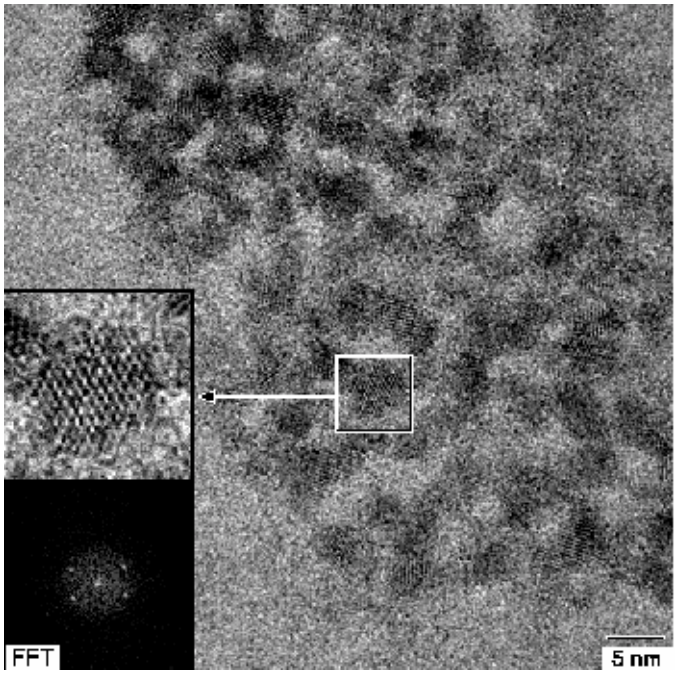

Fig. 3 High-resolution TEM image of HgTe nanocrystals. Inserts show a single HgTe particle with the corresponding FFT.

HgTe particles, high-resolution transmission electron microscopy (HRTEM) images were taken. Figure 3 shows a typical overview image of the sample, together with a micrograph of an individual HgTe particle with a corresponding Fast–Fourier–Transformation (FFT). HRTEM indicates, along with the X-ray diffraction data, a rather broad size distribution of HgTe nanoparticles with sizes ranging from 3 to 6 nm. The existence of the lattice planes on the HRTEM images of the particles indicates a high sample crystallinity. All the images of single particles exhibited an interplanar distance of 3.73 Å belonging to the (111) lattice plane of the coloradoite HgTe phase which, again, is consistent with X-ray diffraction data. P-XRD and HRTEM are today to be considered as standard characterization to be presented in the context of a "new" preparation.

While significant progress has been achieved in controlling the size of nanocrystals, controlling the nanocrystal surface is even more challenging. Because of the high surface-to-volume ratio, the photoluminescence efficiency of nanocrystals can be reduced dramatically by localized surface trap states. Proper surface modification can remove the local trap sites from the surface and thus significantly increase the quantum yield of the near bandgap emission [19–23]. This capping can either be achieved by an inorganic large bandgap material or, as has been shown for CdTe nanoparticles, by the proper choice of the stabilizer [5]. The nanoclusters were prepared in aqueous solution by the reaction between Cd^{2+} and NaHTe in the presence of thioglycolic acid. The photoluminescence strongly depends on the pH value of the colloidal solution and reaches a maximum quantum yield at room temperature of approximately 18% at pH 4.5. Most probably, this pH-dependence is caused by structural changes on the surface. It is suggested that in the acidic range, a shell of cadmium-thiol complexes is formed around the CdTe core.

FURTHER PHOTOPHYSICAL AND STRUCTURAL PROPERTIES

In our first paper on thiol-stabilized CdS particles [1] we pointed out that, as expected from quantum mechanical calculations, the oscillator strength of the 1s-1s excitonic transition increases proportional

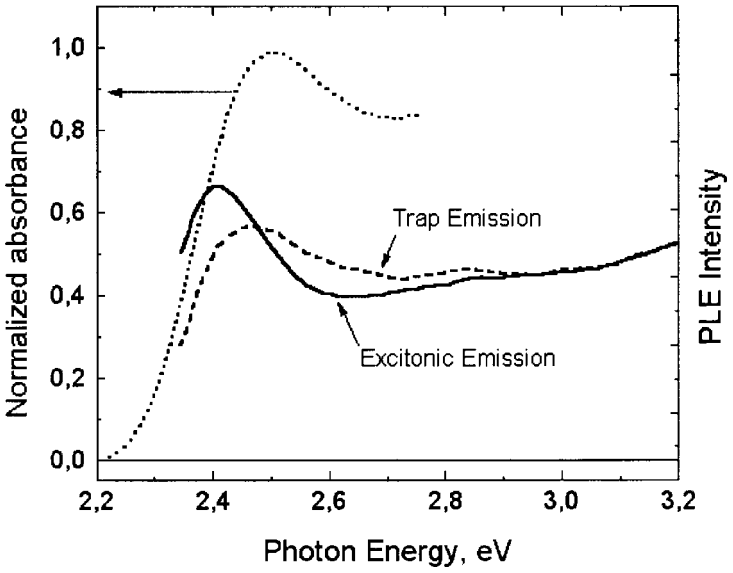

Fig. 4 Room temperature excitation spectra of trap and excitonic emission in CdTe nanocrystals. The absorption spectrum is also displayed for reference.

to $1/r^3$. Furthermore, we observed a particle-size-dependent temperature shift of this transition and a reversible shift of the absorbance when the particles were transferred from their solutions onto quartz substrates and vice versa. The latter observation is still not completely understood and is a matter of current research in our group [24].

Like all other II-VI semiconductor nanocrystals studied so far, thiol-stabilized CdTe particles exhibit quite complex photophysical properties. The luminescence decay kinetics, for example, are strongly nonexponential and are described by extremely broad lifetime distributions lying within the range from a few hundred picoseconds to a few hundred nanoseconds [25]. CdTe nanoclusters (mean diameter $d \sim 2.4$ nm) show both a sharp bandedge luminescence band ($\lambda_{max} \sim 530$ nm) and a wide band of emission via trap states ($\lambda_{max} \sim 635$ nm). The trap luminescence band is substantially quenched when the temperature is increased from 77 to 290 K, which manifests itself in both steady-state emission spectra and luminescence decay kinetics. Figure 4 shows the room temperature excitation spectra for trap emission (dashed line) and excitonic emission (solid line) along with the absorption spectrum (dotted line). The detection energies were chosen at the maxima of the corresponding bands, i. e. 2.294 eV for excitonic emission and 1.936 eV for emission from trap states. Both excitation curves exhibit a similar feature, namely, a low-energy maximum. The fact that the maxima do not coincide means that the absorbed photon should possess a higher energy to excite the trap emission as compared to the exciton luminescence. In ref. 25 three possible explanations for this phenomenon are discussed: i) smaller crystallites whose absorption edge lies at relatively higher energies due to stronger confinement could be responsible for virtually all emission from trap states (like in Cd_3P_2 nanoparticles [26]), ii) there could be two different kinds of particles in the solution: one exhibiting exclusively the exciton luminescence and the other kind having traps at the surface because of incomplete capping giving rise to the red-shifted luminescence, and iii) the inhomogeneous broadening due to the size distribution of the nanocrystals is about 200 meV, which is also a reasonable estimate for the peak width of the excitation spectrum of the excitonic luminescence; the wider band in the excitation spectrum detected within the trap emission could then be associated with an envelope of transitions to higher-lying energy levels.

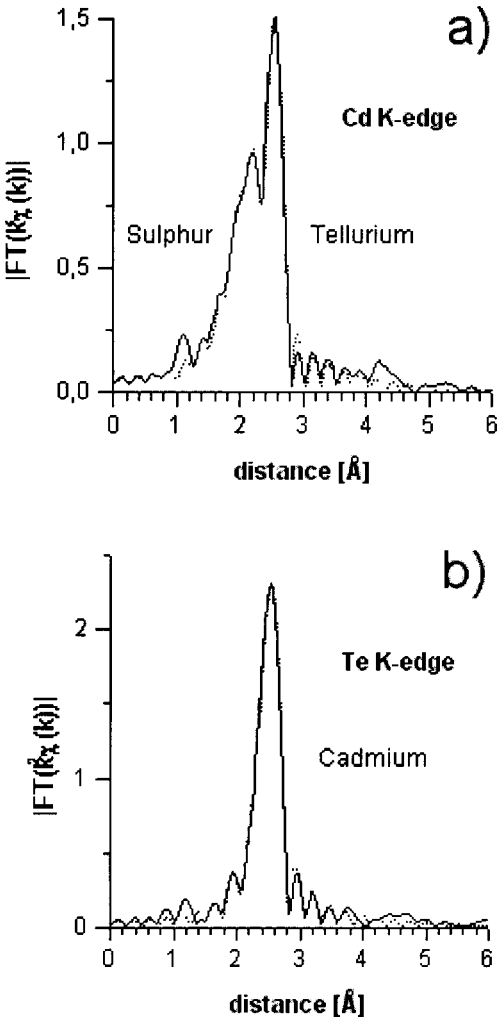

Fig. 5 Fourier transforms (measured curves - solid lines; fits - dashed lines) of the EXAFS spectra of thiol-capped CdTe nanocrystals at 8 K (a) at the Cd K-edge and (b) at the Te K-edge (data ranges of k = 3.5–16.0 $Å^{-1}$ and k = 3.5–15.8 $Å^{-1}$, respectively; sample temperature 8 K).

As has been shown recently on a series of CdS colloids [27] including thiol-stabilized ones and colloidal crystals, EXAFS (Extended X-ray Absorption Fine Structure) provides a valuable tool to determine structural and dynamical properties of nanoclusters. We applied this method also to thiol-capped CdTe nanoparticles in order to investigate the structure and the dynamics of the nanoparticle core and surface separately [28,29]. Figure 5a shows the Fourier transform of the EXAFS spectra of very small thiol-stabilized CdTe nanoparticles taken at the Cd K-edge at 8 K. The observed splitting of the first coordination shell into two contributions clearly indicates that the coordination of the Cd atom consists of Te atoms (from the cluster core) and S atoms (from the ligand shell). In contrast, the respective Fourier transform taken at the Te K-edge shows only one coordination of tellurium which is identified as a Cd shell (Figure 5b). Figure 6 shows the mean interatomic distances $R_{Cd\text{-}X}$ at 8 K of the Cd-Te and Cd-S bonds in the cubic CdTe and hexagonal CdS bulk references and in the nanocrystalline thiol-capped CdTe sample. The interatomic Cd-Te bond distance in CdTe nanoparticles is slightly contracted with respect to the bulk material, whereas a significant expansion of Cd-S bonds is observed. As a consequence of the different bond lengths in macrocrystalline CdTe and in a pure cadmium thiolate ($R_{Cd\text{-}S}$ = 2.540 Å [27]), the heteroepitaxial growth at the core-shell interface causes the experimentally observed lattice contraction of

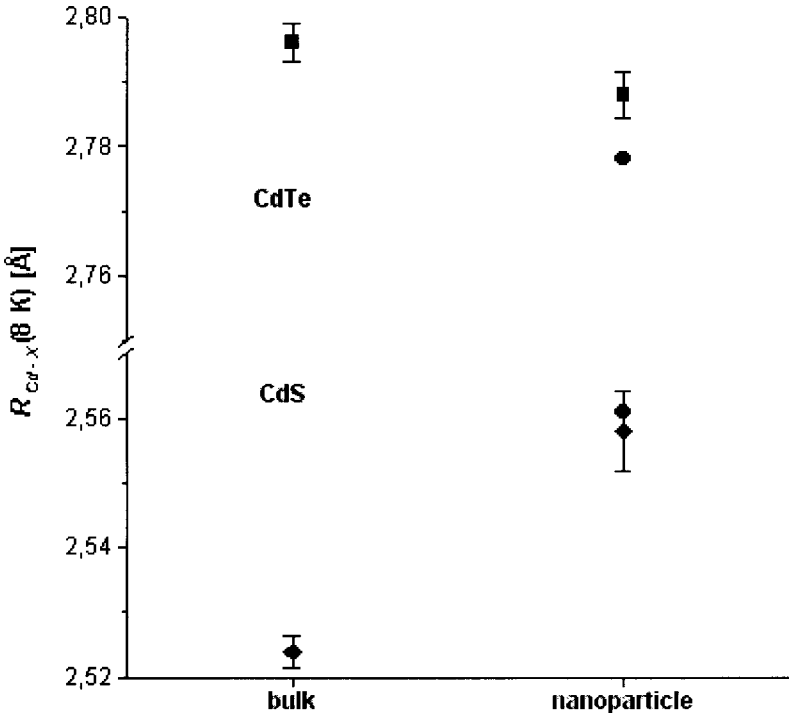

Fig. 6 Mean interatomic distance $R_{Cd\text{-}X}$ of the Cd-Te (squares) and Cd-S (rhombs) bonds in cubic CdTe bulk, hexagonal CdS bulk and thiol-capped CdTe nanocrystals at 8 K. Theoretical Cd-Te and Cd-S bond lengths (circles) calculated with a model accounting for strain distribution in a spherical core-shell system are also shown.

the CdTe particle core and a strong expansion of the Cd-S bond length in the thiolate layer. An isotropic model of elastic strain distribution in a spherical core-shell system of a zincblende CdTe core, heteroepitaxially overgrown by a CdS monolayer describes the experimental results reasonably well (the Cd-Te and Cd-S bond lengths expected from the model are depicted as circles in Fig. 6).

The results of EXAFS measurements on a series of CdS nanocrystals [27] are in agreement with the crystal structures determined by single-crystal X-ray diffraction [15,16]. Since the preparation of thiol-capped CdTe [3] and CdS [1] nanoparticles is very similar, it is obvious to compare the experimental coordination numbers with values expected for Te analogues of CdS nanocrystals with known structure $Cd_{17}S_4(SR)_{26}$ [15] and $Cd_{32}S_{14}(SR)_{36}$ [16]. The difference between the latter two structures is just an additional CdS layer on one tetrahedron face of the $Cd_{17}S_4(SR)_{26}$ cluster. Similarly, the next larger homologue may be constructed by adding another CdS layer to $Cd_{32}S_{14}(SR)_{36}$, resulting in the formula $Cd_{54}S_{32}(SR)_{48}^{4-}$. Replacement of the sulfur atoms in the core of this particle by Te results in the sum formula $Cd_{54}Te_{32}(SCH_2CH_2OH)_{52}^{8-}$. If we assume that the corners in each cluster are fully coordinated by thiols, every Cd atom is coordinated by four Te and/or S. Good agreement between experiment and expectation is observed for this cluster. The structure can be described as a tetrahedron whose edges and corners consist of a Cd-SR surface layer, whereas the particle core and the faces of the tetrahedron are made of CdTe with distorted zincblende lattice. We like to emphasize, however, that this structural suggestion is based on the assumption that the same structural principle of small CdS nanoclusters

holds also in the case of thiol-stabilized CdTe nanoparticles. A clear proof of the real nanocluster structure can only be given by single-crystal X-ray diffraction.

APPLICATIONS

In the final section of this paper, we will briefly outline three examples of what might be called "applications" of semiconductor nanocrystals. Equally well, the terms "use" or "incorporation" could be utilized.

The first example involves the fabrication of 3D colloidal photonic crystals by the self-organization of submicron-sized polystyrene (PS) latex spheres. The latter are covered via consecutive electrostatic adsorption by charged polyelectrolytes and luminescent semiconductor nanocrystals (Fig.7) [30]. CdTe and CdTe(S) nanocrystals [31], capped on the surface with different thiols and sizes ranging from 2.5 to 5 nm, have been prepared with reasonably strong "excitonic" luminescence (6–18% room temperature quantum efficiency (QE)). Nanocrystals stabilized by 1-mercapto-2,3-propandiol and 1,2-dimercapto-3-propanol were found most suitable for their incorporation into polyelectrolyte layers due to the strong electrostatic interactions between the negatively charged –OH and –SH groups on the surface of the nanocrystals and the positively charged polyelectrolytes. Transmission electron microscopy (TEM) confirmed the successful incorporation of the nanocrystals in the polyelectrolyte multilayer shells assembled on the PS latex particles.

The electroluminescence (EL) properties of CdSe nanoparticles embedded in poly(p–phenylene vinylene) have been studied extensively and hybrid organic–inorganic LEDs were realized [32–35] with these structures. We fabricated CdTe nanocrystal/polyaniline composite films [36] as well as films of closely packed CdTe nanocrystals in order to develop a light-emitting device with low turn-on volt-

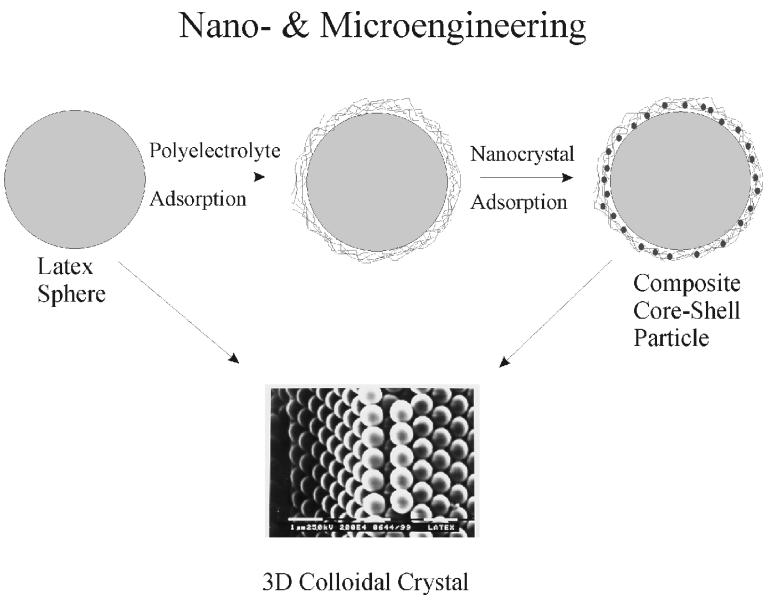

Fig. 7 Schematic illustration of the assembly of polyelectrolytes and luminescent nanocrystals on polystyrene latex spheres and the organization of monodisperse composite particles into a 3D colloidal crystal.

ages. The emitted color of such a device is tunable from green to red depending on the size of the nanocrystals. The use of the particle-loaded polyaniline film as the light-emitting layer results in a considerable enhancement of the quantum efficiency in comparison to the polymer-free device with closely packed CdTe nanocrystals only.

The third example constitutes the use of nanocrystals as potential amplifiers operating at 1.3 μm and 1.55 μm wavelengths for telecommunication devices. Quantum confinement in HgTe quantum dots increases their effective bandgap from close to zero to values above 0.7 eV. Consequently, this material shows infrared luminescence. The room temperature PL emission spectrum of as prepared thiol-stabilized HgTe particles in aqueous solution covers the spectral region from 800 to 1400 nm with a maximum located at 1080 nm and an overall quantum efficiency of approximately 48% for the sample [7]. For efficient laser amplification, the excited state must have a lifetime that is sufficiently long and the material must have a high enough quantum efficiency that significant population inversion over the ground state can occur. To put this in perspective, Rare Earth ions typically have 100 μs - few ms lifetimes and in some cases QEs close to 100%, while in semiconductor lasers, lifetimes may be as short as 10 ns. For thiol-stabilized $Cd_{1-x}Hg_xTe$, the luminescence decay (recorded at 960 nm) was dominated by a single exponential process with a fitted decay time of 130 ns [8]. The 44% QE observed for the $Cd_{1-x}Hg_xTe$ nanocrystals is one of the largest values obtained for the quantum dot class of materials at room temperature. The efficiency is comparable with those of Rare Earth ions in glasses, while the excited state lifetimes are up to an order of magnitude greater than in semiconductor laser devices. These two features together suggest that this type of material is a ready candidate for laser amplifier applications where an easily inverted population of the excited state over the ground state is required.

ACKNOWLEDGMENT

We are deeply indebted to all colleagues who contributed to this work over the past five years. Especially, we wish to mention the members of our groups in Hamburg and Minsk, the British Telecom group of Dr. Mike Burt in Ipswich and the groups of Prof. Helmuth Möhwald, Dr. Sergey Gaponenko and Dr. Larc Tröger in Golm, Minsk and at DESY in Hamburg, respectively. Critical reading of the manuscript by Dr. Markus Haase is gratefully acknowledged. Financial support has been received from the German Science Foundation (DFG), the Volkswagen Stiftung, BT, NATO and INTAS.

REFERENCES

1. T. Voßmeyer, L. Katsikas, M. Giersig, I. G. Popovic, K. Diesner, A. Chemseddine, A. Eychmüller, H. Weller. *J. Phys. Chem.* **98**, 7665–7673 (1994).
2. A. L. Rogach, A. Kornowski, M. Gao, A. Eychmüller, H. Weller. *J. Phys. Chem.* **103**, 3065–3069 (1999).
3. A. L. Rogach, L. Katsikas, A. Kornowski, D. S. Su, A. Eychmüller, H. Weller. *Ber. Bunsenges. Phys. Chem.* **100**, 1772–1778 (1996).
4. A. L. Rogach, L. Katsikas, A. Kornowski, D. Su, A. Eychmüller, H. Weller. *Ber. Bunsenges. Phys. Chem.* **101**, 1668–1670 (1997).
5. M. Gao, S. Kirstein, H. Möhwald, A. L. Rogach, A. Kornowski, A. Eychmüller, H. Weller. *J. Phys. Chem. B* **102**, 8360–8363 (1998).
6. M. T. Harrison, unpublished.
7. A. L. Rogach, S. V. Kershaw, M. Burt, M. Harrison, A. Kornowski, A. Eychmüller, H. Weller. *Adv. Mater.* **11**, 552–555 (1999).
8. S. V. Kershaw, M. Burt, M. Harrison, A. L. Rogach, H. Weller, A. Eychmüller. *Appl. Phys. Lett.* **75**, 1694–1696 (1999).

9. K. Hoppe, A. Kornowski, A. Eychmüller, H. Weller, A. L. Rogach, unpublished.
10. C. B. Murray, D. J. Norris, M. G. Bawendi. *J. Am. Chem. Soc.* **115**, 8706–8715 (1993).
11. O. I. Micic, C. J. Curtis, K. M. Jones, J. R. Sprague, A. J. Nozik. *J. Phys. Chem.* **98**, 4966–4969 (1994).
12. A. Chemseddine, H. Weller. *Ber. Bunsenges. Phys. Chem.* **97**, 636–637 (1993).
13. A. L. Efros, A. L. Efros. *Sov. Phys.-Semiconductors* **16**, 772 (1982).
14. A. I. Ekimov, A. A. Onushchenko. *Sov. Phys.-Semiconductors* **16**, 775 (1982).
15. T. Voßmeyer, G. Reck, L. Katsikas, E. T. K. Haupt, B. Schulz, H. Weller. *Science* **267**, 1476–1479 (1995).
16. T. Voßmeyer, G. Reck, B. Schulz, L. Katsikas, H. Weller. *J. Am. Chem. Soc.* **117**, 12881–12882 (1995).
17. H. Weller, A. Eychmüller, in *Semiconductor Nanoclusters* (P. V.Kamat and D. Meisel, eds.), Vol. 103, p. 5–22. Elsevier Science B. V., Amsterdam, 1996.
18. As mentioned in e.g. J. Rockenberger, A. L. Rogach, M. Tischer, M. Grundmann, H. Weller, A. Eychmüller. *Ber. Bunsenges. Phys. Chem.* **102**, 1561–1564 (1998) the "size" of nanoparticles depends on the method used to determine this quantity.
19. L. Spanhel, M. Haase, H. Weller, A. Henglein. *J. Am. Chem. Soc.* **109**, 5649–5655 (1987).
20. A. Hässelbarth, A. Eychmüller, R. Eichberger, M. Giersig, A. Mews, H. Weller. *J. Phys. Chem.* **97**, 5333–5340 (1993).
21. M. A. Hines, P. Guyot-Sionnest. *J. Phys. Chem.* **100**, 468–471 (1996).
22. B. O. Dabbousi, J. Rodriguez-Viejo, F. V. Mikulec, J. R. Heine, H. Mattoussi, R. Ober, K. F. Jensen, M. B. Bawendi. *J. Phys. Chem. B* **101**, 9436-9475 (1997).
23. X. Peng, M. C. Schlamp, A. V. Kadavanich, A. P. Alivisatos. *J. Am. Chem. Soc.* **119**, 7019–7029 (1997).
24. H. Döllefeld, H. Weller, A. Eychmüller, unpublished.
25. A. M. Kapitonov, A. P. Stupak, S. V. Gaponenko, E. P. Petrov, A. L. Rogach, A. Eychmüller. *J. Phys. Chem. B* **103**, 10109–10113 (1999).
26. A. Kornowski, R. Eichberger, M. Giersig, H. Weller, A. Eychmüller. *J. Phys. Chem.* **100**, 12467–12471 (1996).
27. J. Rockenberger, L. Tröger, A. Kornowski, T. Voßmeyer, A. Eychmüller, J. Feldhaus, H. Weller. *J. Phys. Chem. B* **101**, 2691–2701 (1997).
28. J. Rockenberger, L. Tröger, A. L. Rogach, M. Tischer, M. Grundmann, A. Eychmüller, H. Weller. *J. Chem. Phys.* **108**, 7807–7815 (1997).
29. J. Rockenberger, L. Tröger, A. L. Rogach, M. Tischer, M. Grundmann, H. Weller, A. Eychmüller. *Ber. Bunsenges. Phys. Chem.* **102**, 1561–1564 (1998).
30. A. Rogach, A. Susha, F. Caruso, G. Sukhorukov, A. Kornowski, H. Möhwald, A. Eychmüller, H. Weller. *Adv. Mater.* **12**, 333–337 (2000).
31. A. S. Susha, F. Caruso, A. L. Rogach, G. B. Sukhorukov, A. Kornowski, H. Möhwald, M. Giersig, A. Eychmüller, H. Weller. *Coll. Surf. A* **163**, 39–44 (2000).
32. V. L. Colvin, M. C. Schlamp, A. P. Alivisatos. *Nature* **370**, 354–357 (1994).
33. M. Gao, B. Richter, S. Kirstein. *Adv. Mater.* **9**, 802–805 (1997).
34. M. Gao, B. Richter, S. Kirstein, H. Möhwald. *J. Phys. Chem. B* **102**, 4096–4103 (1998).
35. H. Mattoussi, L. H. Radzilowski, B. O. Dabbousi, E. L. Thomas, M. G. Bawendi, M. F. Rubner. *J. Appl. Phys.* **83**, 7965–7974 (1998).
36. N. P. Gaponik, D. V. Talapin, A. L. Rogach. *Phys. Chem. Chem. Phys.* **1**, 1787–1789 (1999).